Fermi National Accelerator Laboratory

FERMILAB-Conf-89/040

# Strangeness Production in High Energy Proton-Nucleus Collision*

Kam-Biu Luk
Fermi National Accelerator Laboratory
P.O. Box 500, Batavia, Illinois 60510

February 1989

* Invited talk presented at Hadronic Matter in Collision: (Hadron 88), Tucson, Arizona, October 6-12, 1988.

Operated by Universities Research Association, Inc., under contract with the United States Department of Energy

# STRANGENESS PRODUCTION IN HIGH ENERGY PROTON-NUCLEUS COLLISION

Kam-Biu Luk
Fermi National Accelerator Laboratory
P.O.Box 500, Batavia, Illinois 60510

## ABSTRACT

Results on strange particles produced by high energy protons on nuclear targets are reviewed. Topics included are inclusive cross-sections, A-dependence, particle ratios and production polarization of hyperons.

## INTRODUCTION

Inclusive production of strange particles in high energy proton-nucleus collisions is an excellent tool for probing the underlying dynamics of the reactions, and the structure of matter. Being created from the sea, the strange quark can be used to trace the quantum number flow in the collision. By studying how the proton interacts with nuclear matter, we may learn about the space-time development of high energy scatterings at very small distances and short times. Recently, enhanced production of strange particles in relativistic heavy ion collisions is considered as a signature of the formation of quark-gluon plasma.[1,2] Consequently, this triggers new interest in strangeness production in high energy proton-nucleus scatterings.

Experiments studying charged kaon production usually employ a single arm spectrometer with Cerenkov counters for particle identification. The spectrometer is adjusted to detect kaons in certain angular and momentum ranges for a given run. In the case of neutral hyperon experiments, different part of the kinematic region can be investigated by changing the incident angle of the primary protons on target. For charged hyperon experiments, the same goal can be accomplished by tuning the magnetic field in which the hyperon channel is resided, and/or by altering the production angle. In a typical hyperon experiment, hyperons are detected by

observing their decay products. Sometime charged hyperons in the secondary beam can be tagged by a DISC counter. For instance, this was done in the CERN hyperon experiments.[3-5]

In this talk, some properties of single strange particle production in inclusive proton-nucleus reactions are reviewed. Only measurements taken with a proton energy greater than 12 GeV are included. The topics presented are the invariant production cross sections $E(d^3\sigma/dp^3)$, A-dependence, particle ratios and hyperon production polarization. For those who are interested in multiplicity distributions and two particle correlations, the review article by S. Fredriksson et al.[6] should be consulted.

## PRODUCTION CROSS SECTIONS

Differential production cross sections of charged kaons have been extensively measured with different nuclear target materials at various proton energies, up to 400 GeV. Most of the measurements are concentrated in the central region[7-10], and in the beam fragmentation region.[11-17]

With data taken from reference 7, the invariant cross sections of $K^{\pm}$ are plotted as a function of $p_T$ at $90^0$ in the center of mass system in Figures 1a and 1b. The yields tend to increase as the energy of the incident proton is changed from 200 GeV to 400 GeV. At sufficiently high $p_T$, the observed hadron comes from the fragmentation of the interacting partons in the elementary large momentum transfer process. As a result, 'smeared' QCD calculations predict the differential cross section to scale with a form

$$E\frac{d^3\sigma}{dp^3} \approx p_T^m (1 - x_T)^b \qquad (1)$$

where $x_T = 2p_T / \sqrt{s}$, $m = -8$ and $b \approx 9$. As can be seen in Figures 2a and 2b, when $x_T > 0.3$, the measurements for $K^+$ ($K^-$) do scale with $m \approx -8.5$ and $b \approx 7.9$ (11.).

The Feynman $x_F$ dependence of the invariant cross sections of $K^{\pm}$ determined at small $p_T$ with a 6 cm long aluminium target is shown in Figure 3.[15] Comparing with data taken with a thicker target, there is a change in the spectra. In particular, the cross sections can differ by as much as a factor of two at $x = 0.1$. This could be due to intra-nuclear cascade process in the thick target. It is interesting to note that Feynman scaling is observed at proton energy higher than 67 GeV.

Figures 4, 5, 6, 7 and 8 are the production cross sections of $K_s$, neutral hyperons and their anti-particles measured with protons on beryllium at 200, 300 and 400 GeV [18,19,20]. Again, scaling holds for all particles at these energies. There is no data on the production of neutral hyperons with $x_F$ less than 0.2. Since the measurements were performed at fixed production angles, $p_T$ and $x_F$ are correlated. For a given value of $x_F$ the drop in cross section as the production angle increases is simply due to the rapid change of cross section at increasing $p_T$, as can be seen in Figures 9, 10 and 11.[21] When $p_T > 2$ GeV/c, the cross sections also exhibit hard scattering behaviour similar to $K^{\pm}$.

Despite the fact that high energy hyperon beams are now available, data on charged hyperon and anti-hyperon production are still scarce. The only measurement of the invariant cross sections for the charged hyperons at proton energy greater than 200 GeV comes from the CERN Hyperon Group.[3] Their results are shown in Figure 12. In this case, measurements done at BNL or CERN PS energies[5,22] can not be scaled to 200 GeV.

In contrast to high $p_T$ phenomena, for small $p_T$ processes in the beam fragmentation region, particles with sufficiently large $x_F$ are formed by recombining the maximum number of spectator quarks from the beam hadron with the minimum number of other scattered valence quarks or sea partons. Motivated by the quark counting rule in the parton recombination model,[23] it is common to describe the differential cross sections by

$$E\frac{d^3\sigma}{dp^3} \approx (1 - x_F)^n \qquad (2)$$

where n is determined by the quark-interchange process in the transition of the proton to the detected hadron. Table 1 summarizes the measured values of n and the predictions of the quark counting rule. In general, they are in reasonable agreement, except for the anti-hyperons.

## A-DEPENDENCE

The nuclear effect on the differential cross section is intriguing. If a particle produced with high momentum interacts again inside the nucleus, it is expected to emerge with smaller momentum and larger angle. The probability of re-interaction should depend on the number of nucleon available, or the atomic number of the target.

As shown in Figure 13, this speculation is clearly seen in the case of Λ production with beryllium, copper and lead. In general, the differential cross section measured with a nuclear target of atomic number A can be related to that determined with hydrogen by

$$E\frac{d^3\sigma}{dp^3}(A;x_F,p_T) = A^{\alpha(x_F,p_T)}\, E\frac{d^3\sigma}{dp^3}(1;x_F,p_T) \qquad (3)$$

The parameter α has been measured for various particles over a fairly wide range of $x_F$ and $p_T$. The α of the strange particles are shown in Figures 14, 15, 16, 17 and 18. For a given $x_F$, α increases with $p_T$. At some medium $p_T$, for all strange particles, may be except $K_s$, α is even greater than 1. This effect was first discovered by Cronin et al.[24] in 1974 and has been confirmed by many other experiments at different proton energies.[7,8,9,25] The interpretation of this interesting result is that the interacting quark is multiple scattered with the other nucleons in the nucleus before it recombines with other partons, which takes place outside the nucleus, to form the detected hadron.

The energy dependence of α for $K^{\pm}$ is shown in Figure 19, taken from reference 7. At small $p_T$ in the central region, α grows with the incident proton energy, but it decreases slowly or is almost flat at medium $p_T$.

Comparison of α integrated over $p_T$ for the neutral strange particles is given in Figure 20. The general trends are the same, $\alpha(x_F)$ decreases from a value of 0.75 at $x_F = 0.2$ to a value of 0.45 at $x_F = 0.8$, and $\alpha(x_F)$ of $\Xi^0$ tends to be systematically larger than the others.

## PARTICLE RATIOS

Particle ratios can be used to examine the relative dependence of Bjorken x of the structure functions of those partons which take part in the hadronization process. For example, $K^+$ is made up of a constituent u quark from the incident proton and a $\bar{s}$ quark from the sea whereas $\pi^+$ is a product of a valence u quark and a sea $\bar{d}$. The ratio $K^+/\pi^+ \sim \bar{s}(x)/\bar{d}(x)$ reflects strangeness suppression in the fragmentation process. In the case of $K^-$, it does not contain any valence quarks in common with the proton, the ratio $K^-/\pi^-$ will allow us to determine how the $K^-$ is formed.

Taken from reference 26, figures 21, 22 show the ratios of $K^{\pm}/\pi^{\pm}$, measured with an aluminium target, as a function of $x_F$ and $p_T$. Both ratios satisfy Feynman

scaling when the primary proton energy is greater than 67 GeV. At $x_F = 0.1$, up to $p_T$ of 0.5 GeV/c, $K^{\pm}/\pi^{\pm}$ are flat in $p_T$, with $K^+/\pi^+ \approx 0.1$ and $K^-/\pi^- \approx 0.08$. With beryllium and aluminium targets, Bozzoli et al.[27] also saw a similar behaviour between rapidity y = 1.4 and y = 2.1 at zero $p_T$.

The ratios $K^{\pm}/\pi^{\pm}$ have also been determined with $p_T$ out to 10 GeV/c at $90^0$ in the center of mass system. The preliminary results from Fermilab E605 with 800 GeV protons on beryllium[28] are compared with the CP data,[7] along with the ISR measurements,[29] in Figures 23 and 24. When $p_T < 2.5$ GeV/c, both ratios increase with $p_T$. Beyond this point, $K^+/\pi^+$ reaches a value of 0.5 and stays constant, indpendent of $\sqrt{s}$, center of mass angle or type of reaction. Then it seems to start to drop at $p_T > 10$ GeV/c. However, there are not enough data to investigate the trend. On the other hand, $K^-/\pi^-$ shows a very different kind of picture. After attaining its maximum value at $p_T \approx 3$ GeV/c, it gradually reduces with $p_T$. Furthermore, the ABCDHW results at $\theta_{cm} = 50^0$ are consistently higher than the E605 and CP measurements. This may be due to the fact that the experiments are probing different kinematic domains.

The A-dependence of $K^{\pm}/\pi^{\pm}$ ratios at 400 GeV is given in Figure 25.[7] At low $p_T$, the difference $\alpha_K - \alpha_\pi$ tends to increase and approaches a value of 0.1. In other words, $K^{\pm}$ are more abundantly produced than $\pi^{\pm}$ with higher A targets. This may imply that in high energy heavy ion collisions, disregarding whether quark-gluon plasma is formed, we should see an enhancement in the ratios of $K^{\pm}/\pi^{\pm}$ with respect to the ordinary proton-nucleus reactions.

The ratios of charged hyperons to $\pi^{\pm}$ have only be determined at 200, 210, 240 and 400 GeV.[3,4,30] As can be seen in Figures 26a and 26b, all ratios increase with $x_F$. This means, in general, baryons are produced stiffer than mesons in proton induced processes. In addition, the $\Sigma^{\pm}/\pi^{\pm}$ ratios are insenitive to $p_T$. The other ratios are harder to conclude because of limited statistics. Furthermore, the 400 GeV measurements are consistent with the CERN observations at $x_F = 0.48$ and small $p_T$.

In Figure 27, taken from reference 19, the ratio $K_S/\Lambda$ is independent of the target material and production angle, that is $p_T$, between $x_F$ of 0.2 and 0.8.

It is well known that a large fraction of the stable low mass strange particles are not directly produced.[23] They are mostly decay products of other particles or resonances. To illustrate this point, Figure 28 shows the ratio of $\Lambda(\Sigma^0)/\Lambda$.[31] The ratio is constant at 0.25 and does not change with $p_T$. This has a far-reaching implication on the production polarization of $\Lambda$ which will be presented in the next section.

Another interesting quantity is the ratio of anti-particle to particle. Presumably

it is equally likely to create a particle or an anti-particle with low transverse momentum in the central region in high energy collisions. Consequently, the ratio is expected to be one. On the other hand, if a particle that contains at least one common quark from the incident hadron, the anti-particle to particle ratio should shrink with $x_F$. This reflects the fact that the sea partons have a softer distribution in Bjorken x than the valence quark.

Figure 29 shows the $K^-/K^+$ ratio at low $p_T$. As expected, the ratio reduces by an order of magnitude between $x_F = 0.1$ and $x_F = 0.7$. Furthermore, it depends weakly on the incident proton energy. From Figure 14, we can infer that the $K^-/K^+$ ratio in the central region gets larger with $p_T$ and the atomic number of the target. This distinct feature is not shared by the $\pi^-/\pi^+$ or $\bar{p}/p$ ratios.

The ratio of $\overline{\Lambda}/\Lambda$ has been measured at BNL energy[32] and at Fermilab energies.[19-21] On the other hand, there is only one study of $\overline{\Xi}^0/\Xi^0$.[20] In the region of the measurements, as seen in Figures 30 and 31, both ratios do not have any sign of $p_T$ dependence. Furthermore, $\overline{\Lambda}/\Lambda$ scales with the proton energy. We may tempt to predict $\overline{\Lambda}/\Lambda$ be unity at $x_F = 0$ by extrapolation. However, compilation of experimental results from proton-proton and neutron-nucleus collisions at different energies indicates that $\overline{\Lambda}/\Lambda$ is only asymptotically approaching one at $x_F$=0 at very high energy, as shown in Figure 32.[33] This essentially reflects the grow of the total production section of $\overline{\Lambda}$.[34]

For the charged hyperon sector, the most surprising result is the ratio of $\overline{\Omega}^+/\Omega^-$. Since both of them do not inherit any valence quarks from the incident proton, they are expected to be created with equal probability. Instead, a value of 0.28 was found at $x_F$=0.48 and small $p_T$.[4] Recently, Fermilab E756 has collected a large sample of charged hyperons and anti-hyperons which were produced by 800 GeV protons on beryllium at 2.5 mrad. Some of the preliminary results on particle ratios, based on a small fraction of the data set, are shown in Figures 33 and 34. The striking result on $\overline{\Omega}^+/\Omega^-$ discovered by the CERN Hyperon Group is confirmed. Information on anti-particle to particle ratios at $x_F = 0.48$ is summarized in Figure 35. The general trend is the ratio increases with strangeness.

It is interesting to point out that, within errors, ratios $\overline{\Xi}^0/\Xi^0$ and $\overline{\Xi}^+/\Xi^-$ are identical through out the entire $x_F$ region covered by experiments. This implies, at quark level, $\bar{u}(x)/u(x)$ and $\bar{d}(x)/d(x)$ have the same probability distributions.

Another intriguing preliminary result from E756 is the $\Omega^-/\Xi^-$ ratio which is shown in Figure 36. Despite the fact that we have to extract three quarks from the sea

in order to form an $\Omega^-$ or an $\bar{\Xi}^+$, comparison of $\Omega^-/\Xi^-$ with $\bar{\Xi}^+/\Xi^-$ indicates the $\Omega^-$ behaves like a leading baryon with a fairly stiff production spectrum.

## HYPERON PRODUCTION POLARIZATION

The unexpected discovery of sizable polarization of $\Lambda$'s inclusively produced in unpolarized proton-beryllium reactions at Fermilab[35] has been confirmed and extensively studied by a series of experiments performed from 12 GeV up to ISR energies.[21,32,36-39] As shown in Figures 37, 38 and 39, the general features of this phenomenon can be summarized as follows:

(i) The polarization is normal to the production plane, as required by parity conservation in strong interactions.

(i) The polarization is insensitive to the incident proton energy.

(ii) It is not a nuclear effect.

(iii) For $p_T$ less than 1 GeV/c, the magnitude of the polarization increases with $p_T$ and depends weakly on $x_F$. When $p_T$ is larger than 1 GeV/c, the kinematic behaviour is reversed; the polarization is only a function of $x_F$ and remains constant up to $p_T$ of 3.5 GeV/c.[21]

(iv) The absolute value of the polarization decreases as the atomic number of the target increases.[21,38,39]

As we have pointed out that a large fraction of the detected $\Lambda$'s comes from the decays of $\Sigma^0$'s. Since the daughter $\Lambda$'s preserve on the average -1/3 of the $\Sigma^0$ polarization, the intrinic polarization of the prompt $\Lambda$'s could actually be larger than what is observed in the experiments.

The polarization study has been extended to all long lived hyperons[40-45] as well as $\Sigma^0$ [46] and $\bar{\Lambda}$.[21,35,38] The results are summarized in Figure 40. The polarizations of $\Xi$'s are similar to that of $\Lambda$ whereas $\Sigma$'s are opposite. $\bar{\Lambda}$ is unpolarized up to $p_T$ of 2.5 GeV/c. It should be mentioned that both $\Omega^-$ and $\bar{\Lambda}$ do not carry any valence quark of the incident proton. Yet, the invariant cross section of $\Omega^-$ looks very different from the production spectrum of $\bar{\Lambda}$ in the same kinematic region. On the other hand, production of $\Omega^-$ resembles that of $\Xi^-$ which is known to be polarized. Naively, we might expect $\Omega^-$ to be polarized in a similar fashion. However, as shown in Figure 41, preliminary result from E756 indicates, when produced by proton, the polarization of $\Omega^-$ is small if not zero. A tentative explanation is that strange quarks are not produced polarized. The observed hyperon

polarization is related to the recombination of strange quark(s) with the spectator quark(s). If there is no spectator quark in the emerging hyperon, its polarization will tend to be small.

There are theoretical attempts in explaining the hyperon polarization phenonemon.[47-49] Unfortunately, none of them can quantitatively describe the experimental data. The only empirical rule is that, in the process of recombination, the leading spectator(s) prefers to have the spin pointing 'up' and the slowly moving parton(s) from the sea will tend to have the spin 'down'. This simple rule, probably related to the structure of the SU(6) wavefunctions of hadrons, can be used to explain the sign of the polarization. For example, in the production of $\Sigma^+$, the spin-1 (uu)-diquark will tend to have a spin projection $m_z = 1$ whereas $m_z$ of the s-quark is -1/2. Consequently, the polarization of $\Sigma^+$ is positive.

## CONCLUSIONS

Except for $K^{\pm}$, comprehensive study of strange particle production in high energy proton-nucleus collisions is still lacking. In particular, there is no information on hyperon and anti-hyperon production with $p_T$ less than 1 GeV/c and $x_F$ less than 0.2. Furthermore, not much is known about strangeness production in the target fragmentation region. In order to understanding what is going on in relativistic nucleus-nulceus collisions, it is important to determine the differential cross section of $\pi^-$ and as many particle ratios as possible over a broad range of kinematic region, using different target materials and projectiles at different energies. After all, extrapolation from existing measurements to other unexplored kinematic region sometime could be unreliable and could lead to wrong conclusions.

## ACKNOWLEDGEMENTS

I would like to thank Johann Rafelski for the invitation to this interesting conference. This research was supported by the U.S. Department of Energy.

## REFERENCES

1. P. Koch, Z. Phys. C38, 269(1988); N. K. Glendenning, J. Rafelski, Phys. Rev. C31, 823(1985); J. Kapusta, A. Mekjian, Phys. Rev. D33, 1304(1986);

T. Matsui, B. Svetitsky, L. D. McLerran, Phys. Rev. D34, 783, 3047(1986); K. Kajantie, M. Kataja, P. V. Ruuskanen, Phys. Lett. B179, 153(1986).

2. P. Koch et al., Mod. Phys. Lett. A3, 737(1988); P. Koch, B. Muller, J. Rafelski, Phys. Rep. 142C, 167(1986).
3. M. Bourquin et al., Nucl. Phys. B153, 13(1979).
4. M. Bourquin et al., Z. Phys. C5, 275(1980).
5. J. Badier et al., Phys. Lett. 39B, 414(1972).
6. S. Fredriksson et al., Phys. Rep. 144C, 187(1987).
7. D. Antreasyan et al., Phys. Rev. D19, 764(1979).
8. V. V. Abramov et al., Z. Phys. C24, 205(1984); V. V. Abramov et al., Sov. J. Nucl. Phys. 41, 227(1985).
9. U. Becker et al., Phys. Rev. Lett. 37, 1731(1976).
10. A. Bamberger et al., Nuo. Cim. 62A, 327(1981).
11. D. Dekkers et al., Phys. Rev. B137, 962(1965).
12. T. Eichten et al., Nucl. Phys. B44, 333(1972).
13. J. V. Allaby et al., Preprint CERN 70-12(1970).
14. D. S. Barton et al., Phys. Rev. D27, 2580(1983).
15. N. I. Bozhko et al., Sov. J. Nuc. Phys. 31, 644(1980); N. I. Bozhko et al., Sov. J. Nuc. Phys. 31, 775(1980).
16. B. Aubert et al., Preprint Fermilab-Conf-75/31-EXP.
17. H. W. Atheron et al., CERN Yellow Report CERN-80-07(1980).
18. R. T. Edwards et al., Phys. Rev. D18, 76(1978).
19. P. Skubic et al., Phys. Rev. D18, 3115(1978).
20. A. Beretvas et al., Phys. Rev. D34, 53(1986).
21. B. G. Lundberg, Ph. D. thesis, University of Wisconsin, Madison (1984).
22. V. Hungerbuhler et al., Phys. Rev. D12, 1203(1975).
23. See, for example, K. Fialkowski and W. Kittel, Rep. Prog. Phys. 46, 1283(1983); references contained therein.
24. J.W. Cronin et al., Phys. Rev. D11, 3105(1975).
25. D. A. Garbutt et al., Phys. Lett. 67B, 355(1977).
26. N. I. Bozhko et al., Sov. J. Nucl. Phys. 29, 345(1979).
27. W. Bozzoli et al., Nucl. Phys. B140, 271(1978).
28. P. B. Straub, Ph. D. thesis, University of Washington, Seattle (1989).
29. A. Breakstone et al., Z. Phys. C27, 205(1985).
30. T. R. Cardello et al., Phys. Rev. D32, 1(1985).

31. M. W. Sullivan et al., Phys. Rev. D36, 674(1987).
32. K. Rayachauduri et al., Phys. Lett. 90B, 319(1980).
33. J. Enagonio, Ph. D. thesis, University of Colorado, Boulder(1987).
34. F. W. Busser et al., Phys. Lett. 61B, 309(1976).
35. G. Bunce et al., Phys. Rev. Lett. 36, 1113(1976).
36. S. Erhan et al., Phys. Lett. 82B, 301(1979).
37. F. Lomanno et al., Phys. Lett. 96B, 223(1980).
38. K. Heller et al., Phys. Rev. Lett. 51, 2025(1983).
39. F. Abe et al., Phys. Rev. Lett. 50, 1102(1983); F. Abe et al., J. Phys. Soc. Jpn. 52, 4107(1983).
40. C. Wilkinson et al., Phys. Rev. Lett. 46, 803(1981).
41. L. Deck et al., Phys. Rev. D28, 1(1983).
42. R. Rameika et al., Phys. Rev. D33, 3172(1986).
43. Y. W. Wah et al., Phys. Rev. Lett. 55, 2551(1985).
44. G. Zapalac et al., Phys. Rev. Lett. 57, 1526(1986).
45. C. Ankenbrandt et al., Phys. Rev. Lett. 51, 863(1983).
46. E. C. Dukes et al., Phys. Lett. 193B, 135(1987).
47. T. A. DeGrand and H. I. Miettinen, Phys. Rev. D24, 2419(1981); ibid. D31, 661(E) (1985).
48. T. A. DeGrand, J. Markkanen and H. I. Miettinen, Phys. Rev. D32, 2445(1985).
49. B. Anderson, G. Gustafson and G. Ingelman, Phys. Lett. 85B, 417(1979).

Table 1 Comparison of measured values of the exponent n in the parametrization $E(d^3\sigma/dp^3) \approx (1-x_F)^n$ with the predictions of the quark counting rule for strange particle production by protons at $p_T = 0$. Note A-dependence of the invariant cross section can affect the measure values.

| Particle | measured | prediction |
|---|---|---|
| $K^+$ | 2.5 | 3 |
| $K^-$ | 5.6 | 5 |
| $K^0$ | 2.2 | 4 |
| $\Lambda$ | 0.9 | 1 |
| $\overline{\Lambda}$ | 8.4 | 5 |
| $\Sigma^+$ | 1.5 | 1 |
| $\Sigma^-$ | 3 | 4 |
| $\Xi^0$ | 3 | 4 |
| $\overline{\Xi}^0$ | 11 | 5 |
| $\Xi^-$ | 3 | 4 |
| $\Omega^-$ | 5 | 5 |

## FIGURE CAPTIONS

Figure 1a $E(d^3\sigma/dp^3)$ as a function of $p_T$ at $90^0$ in center of mass system for $K^+$ in pW collisions.

Figure 1b $E(d^3\sigma/dp^3)$ as a function of $p_T$ at $90^0$ in center of mass system for $K^-$ in pW collisions.

Figure 2a $p_T^{8.5}E(d^3\sigma/dp^3)$ versus $x_T$ at $90^0$ in center of mass system for $K^+$ in pW collisions.

Figure 2b $p_T^{8.5}E(d^3\sigma/dp^3)$ versus $x_T$ at $90^0$ in center of mass system for $K^-$ in pW collisions.

Figure 3 $E(d^3\sigma/dp^3)$ versus $x_F$ at low $p_T$ for $K^\pm$ in pAl collisions. Solid curves show results at 19.2 GeV/c and dashed curves at 300 GeV/c.

Figure 4 $E(d^3\sigma/dp^3)$ versus $x_F$ at zero $p_T$ for $K_s$ in pBe collisions.

Figure 5 $E(d^3\sigma/dp^3)$ versus $x_F$ at zero $p_T$ for $\Lambda$ in pBe collisions.

Figure 6 $E(d^3\sigma/dp^3)$ versus $x_F$ at zero $p_T$ for $\overline{\Lambda}$ in pBe collisions.

Figure 7 $(E/\sigma)(d^3\sigma/dp^3)$ versus $x_F$ for $\Xi^0$ in pBe collisions, $\sigma$ = 216 mb, taken from reference 20.

Figure 8 $E(d^3\sigma/dp^3)$ versus $x_F$ for $\overline{\Xi}^0$ in pBe collisions, taken from reference 20.

Figure 9 $E(d^3\sigma/dp^3)$ versus $p_T$ for $K_s$ in pBe collisions, taken from reference 21. Solid lines are empirical fits to data.

Figure 10 $E(d^3\sigma/dp^3)$ versus $p_T$ for $\Lambda$ in pBe collisions, taken from reference 21. Solid lines are empirical fits to data.

Figure 11 $E(d^3\sigma/dp^3)$ versus $p_T$ for $\overline{\Lambda}$ in pBe collisions, taken from reference 21. Solid lines are empirical fits to data.

Figure 12 $E(d^3\sigma/dp^3)$ versus $x_F$ at small $p_T$ for charged hyperons in pBe collisions, taken from reference 3. Solid lines are parametizations of the form $(1-x_F)^n$.

Figure 13 Comparison of $\Lambda$ production in p-nuleus collisions.

Figure 14 Exponent $\alpha$ for $K^\pm$ in proton induced reactions in proton induced reactions. Taken from reference 7.

Figure 15 Exponent $\alpha(x_F,p_T)$ for $K_s$ in proton induced reactions.

Figure 16 Exponent $\alpha(x_F,p_T)$ for $\underline{\Lambda}$ in proton induced reactions.

Figure 17 Exponent $\alpha(x_F,p_T)$ for $\overline{\Lambda}$ in proton induced reactions.

Figure 18 Exponent $\alpha(x_F,p_T)$ for $\Xi^0$ in proton induced reactions, taken from reference 20. Solid lines are empirical fits to data.

Figure 19 Energy dependence of exponent $\alpha$ in proton induced reactions, taken from reference 7. Points with open circles are for $p_T$ = 0.77GeV/c, with closed circles are for $p_T$ = 3.08 GeV/c, and open squares for $p_T$ = 4.62 GeV/c.

Figure 20 Exponent $\alpha(x_F)$ for neutral strange particles in proton induced reactions, taken from reference 20.

Figure 21 Ratios $K^\pm/\pi^\pm$ as a function of $x_F$, taken from reference 26. Solid curves are results at Fermilab energies and dashed curves are from CERN PS.

Figure 22 Ratios $K^{\pm}/\pi^{\pm}$ as a function of $p_T$, taken from reference 26. Solid curves are results at Fermilab energies and dashed curves are from CERN PS.

Figure 23 Ratio $K^+/\pi^+$ versus $p_T$.

Figure 24 Ratio $K^-/\pi^-$ versus $p_T$.

Figure 25 A-dependence of ratios $K^{\pm}/\pi^{\pm}$ in 400 GeV proton induced reactions, taken from reference 7.

Figure 26a Ratios of charged hyperons to $\pi^-$ as a function of $x_F$ at 400 GeV/c, taken from reference 30. Solid curves are fits of the form $(1-x_F)^n$.

Figure 26b Ratios of charged hyperons to $\pi^+$ as a function of $x_F$ at 400 GeV/c, taken from reference 30. Solid curves are fits of the form $(1-x_F)^n$.

Figure 27 Ratio of $K_s/\Lambda$ measured in 300 GeV proton (a) beryllium, (b) lead collisions, taken from reference 19.

Figure 28 Ratio of $\Lambda$ from $\Sigma^0$ decays to all detected $\Lambda$ in proton-beryllium reacions at BNL energy, taken from reference 31.

Figure 29 Ratio of $K^+$ to $K^-$ versus $x_F$ at low $p_T$ in proton-aluminium interactions, taken from reference 26.

Figure 30 Ratio of $\overline{\Lambda}$ to $\Lambda$ in 400 GeV p-Be reactions, taken from reference 20. Solid line is the fit to 300 GeV data.

Figure 31 Ratio of $\overline{\Xi}^0$ to $\Xi^0$ in 400 GeV p-Be reactions, taken from reference 20.

Figure 32 Ratio of $\overline{\Lambda}$ to $\Lambda$ versus $\sqrt{s}$ at $x_F = 0$.

Figure 33 Preliminary results from Fermilab E756 on the ratio of $\overline{\Xi}^+/\Xi^-$ as a function of $x_F$ at 2.5mrad in 800 GeV proton beryllium collisions.

Figure 34 Preliminary results from Fermilab E756 on the ratio of $\overline{\Omega}^+/\Omega^-$ as a function of $x_F$ at 2.5mrad in 800 GeV proton beryllium collisions.

Figure 35 Ratios of anti-particle to particle as a function of strangeness.

Figure 36 Preliminary results from Fermilab E756 on the ratio of $\Omega^-/\Xi^-$ as a function of $x_F$ at 2.5mrad in 800 GeV proton beryllium collisions.

Figure 37 Energy dependence of $\Lambda$ production polarization.

Figure 38 Polarization of $\Lambda$ versus $p_T$.

Figure 39 A-dependence of polarization of $\Lambda$.

Figure 40 Polarization of hyperons in proton induced reactions.

Figure 41 Preliminary results from E756 on polarizations of $\Omega^-$ and $\Xi^-$ in 800 GeV proton beryllium interactions.

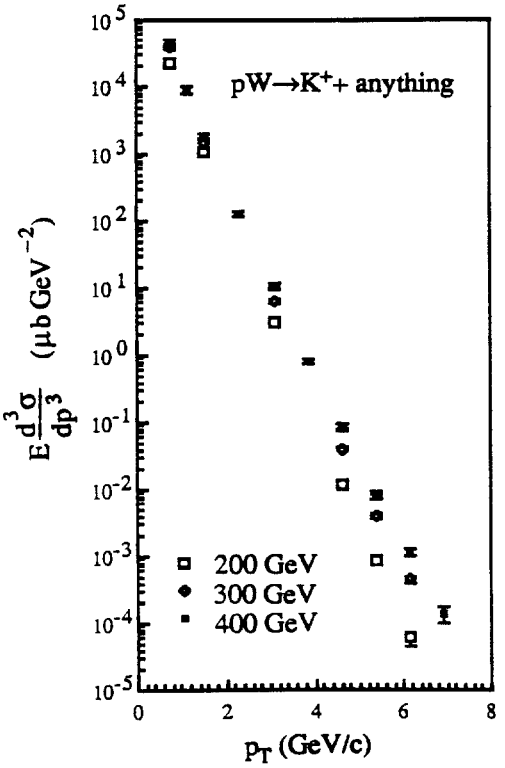


Figure 1a

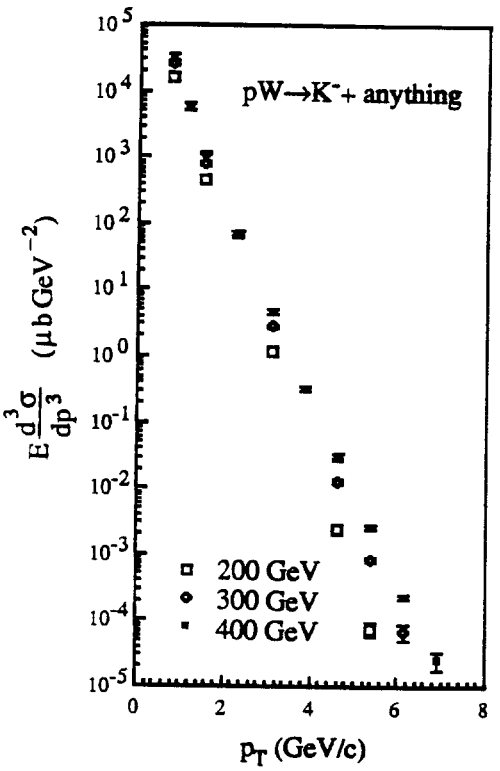


Figure 1b

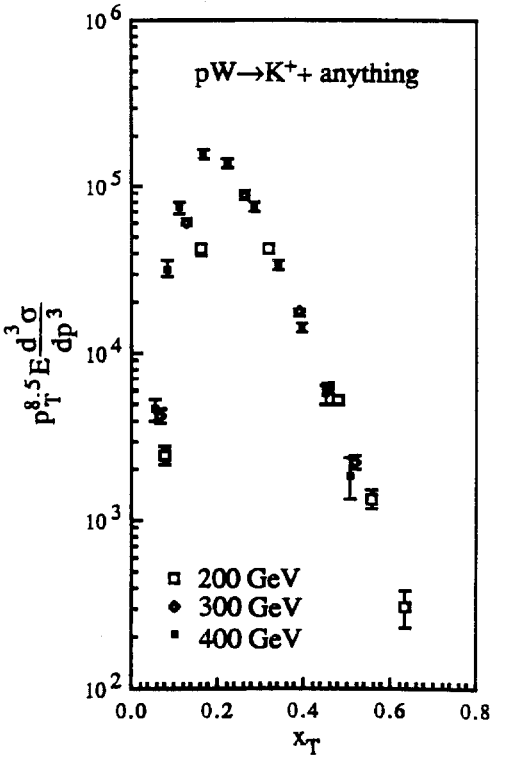


Figure 2a

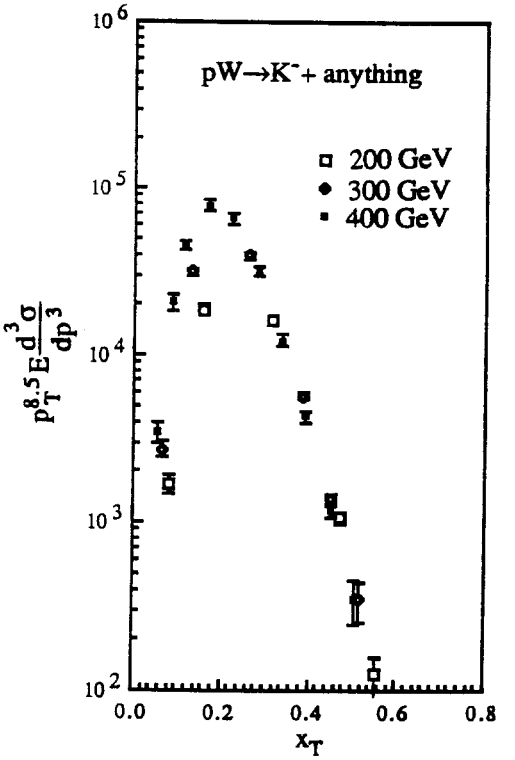


Figure 2b

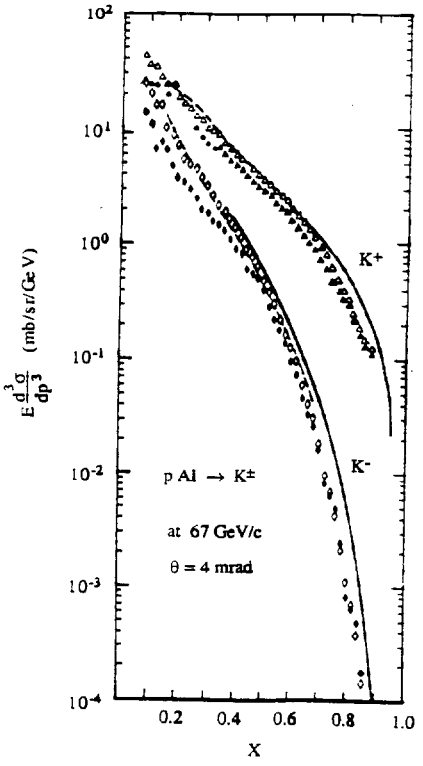


Figure 3

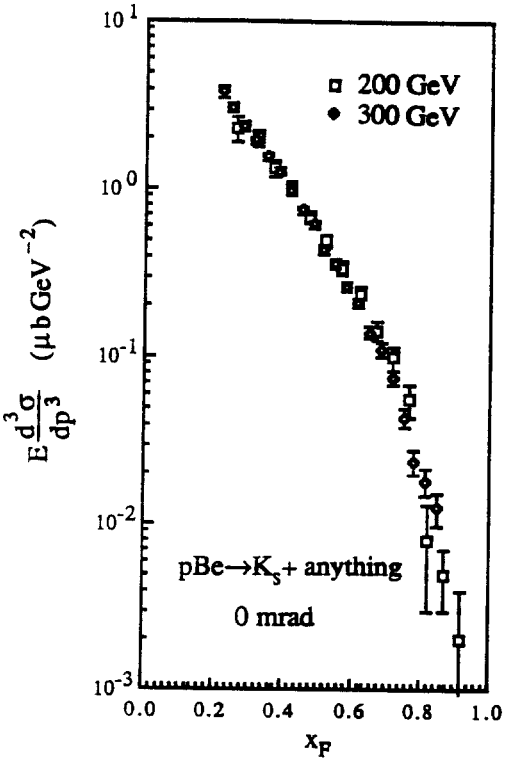


Figure 4

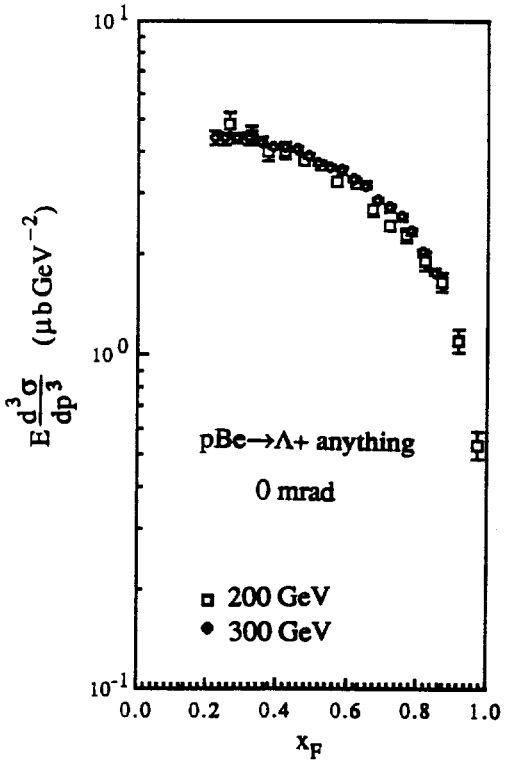


Figure 5

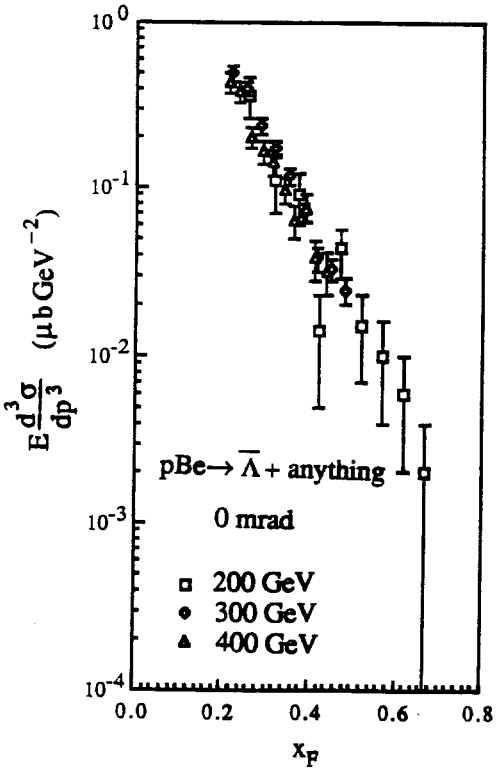


Figure 6

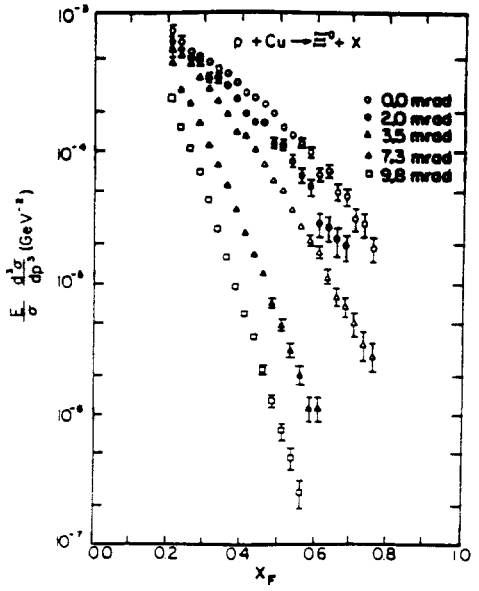


Figure 7

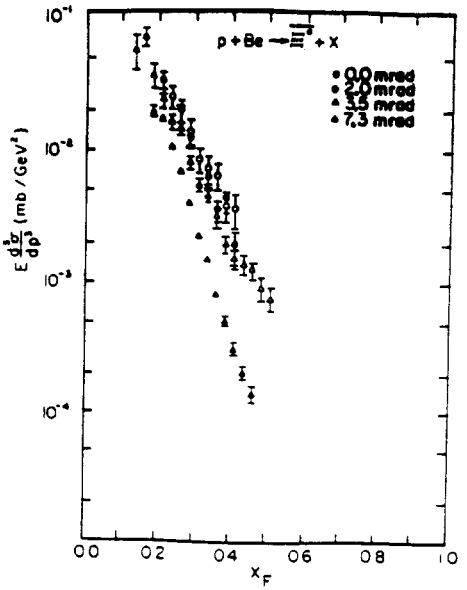


Figure 8

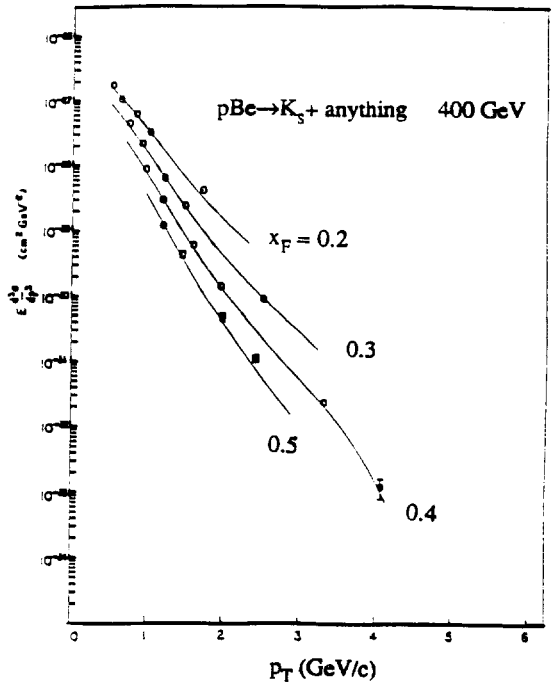


Figure 9

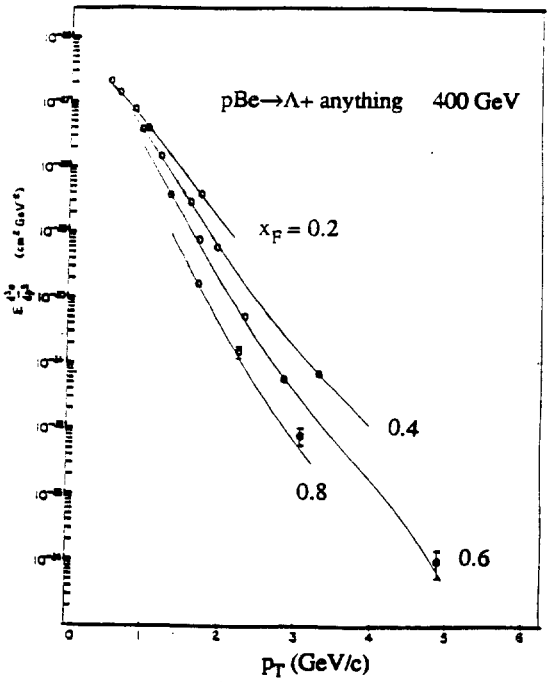


Figure 10

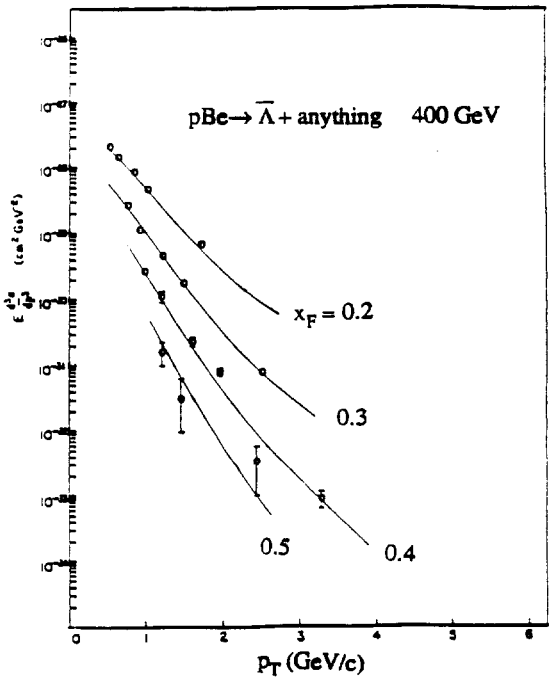


Figure 11

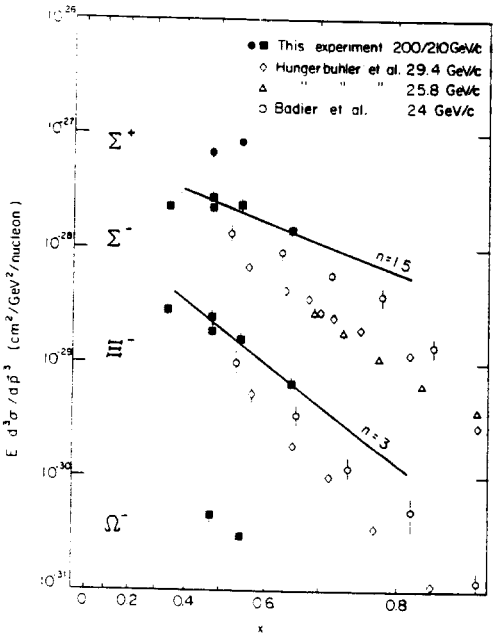


Figure 12

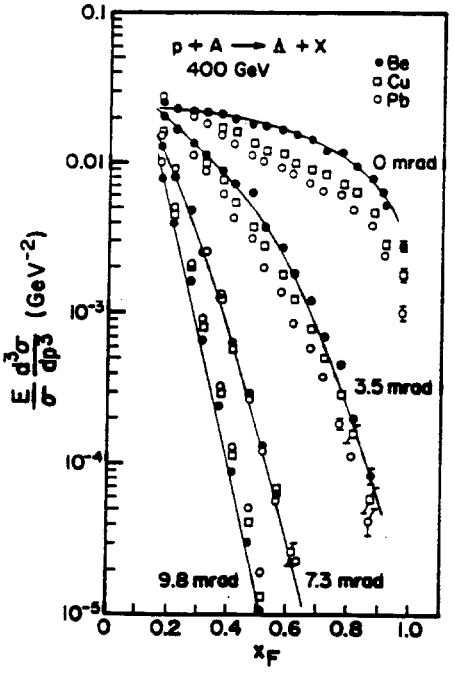


Figure 13

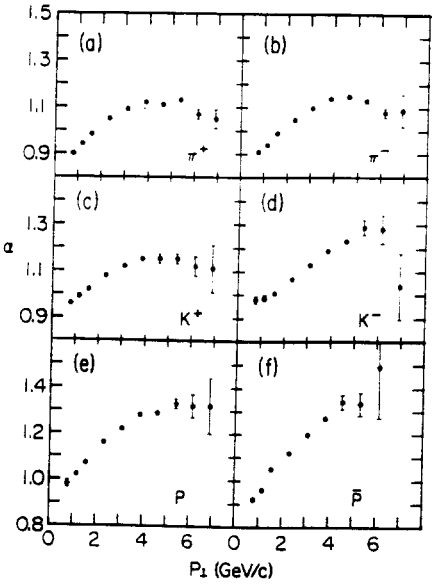


Figure 14

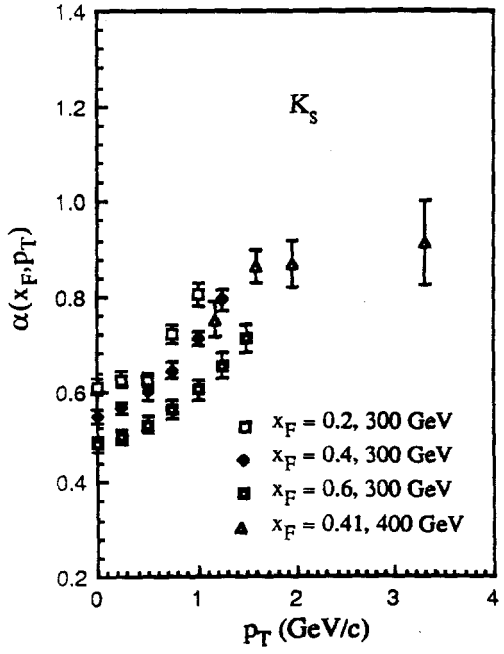


Figure 15

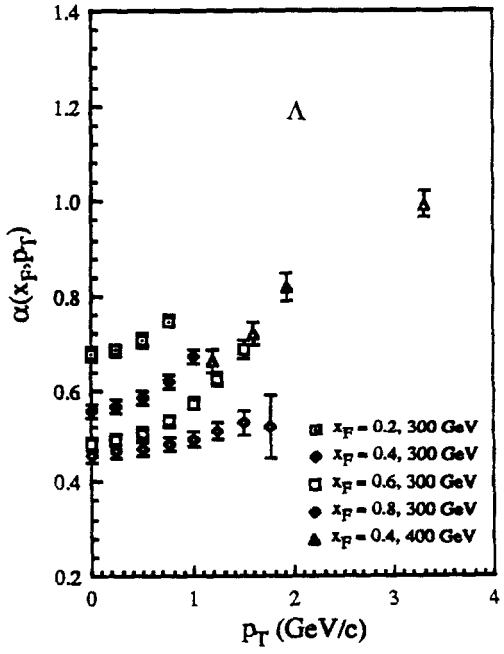


Figure 16

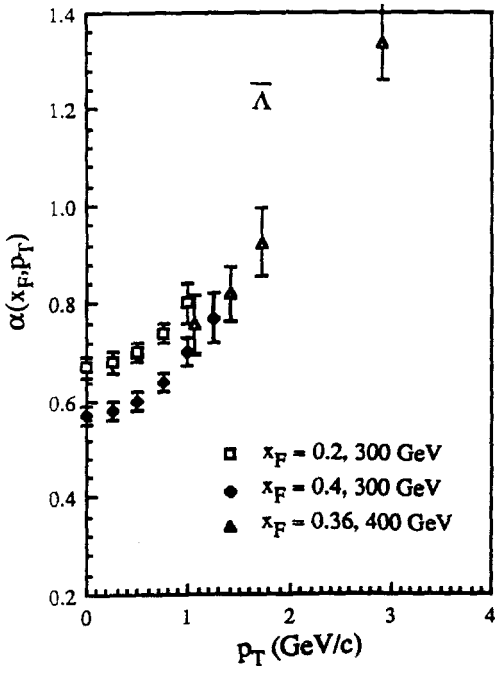


Figure 17

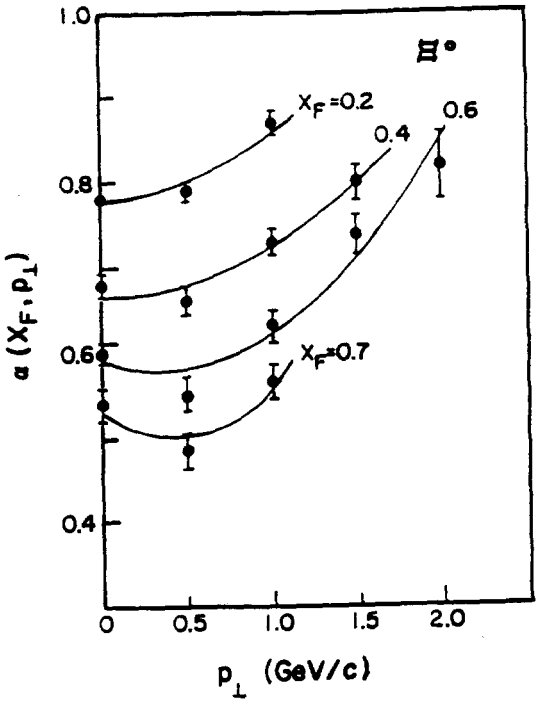


Figure 18

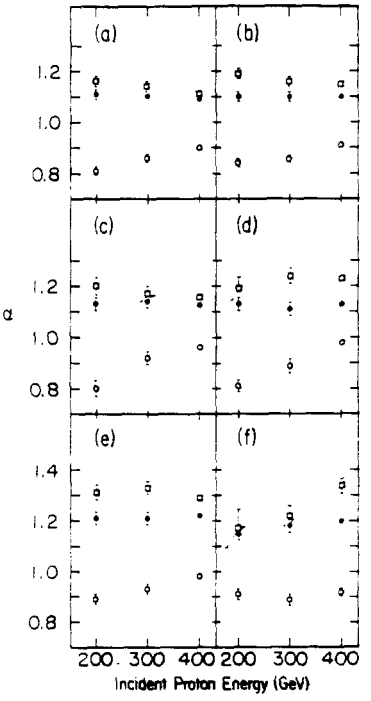


Figure 19

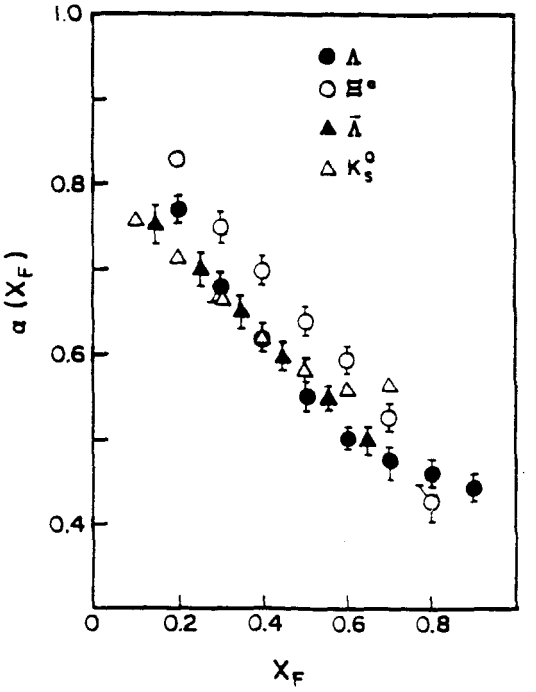


Figure 20

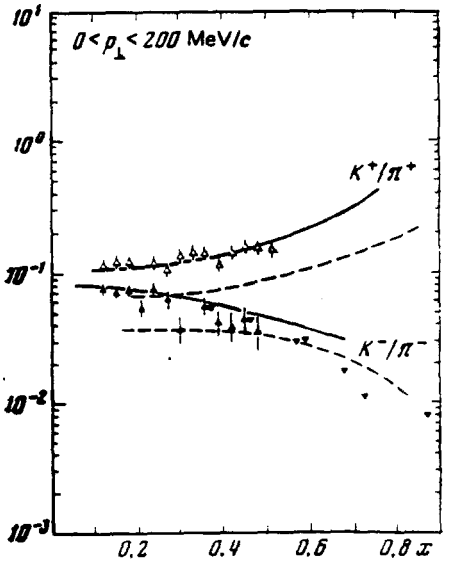


Figure 21

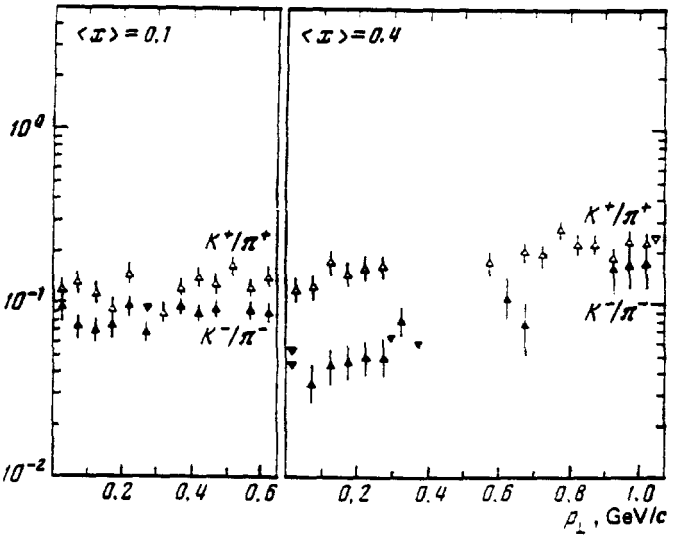


Figure 22

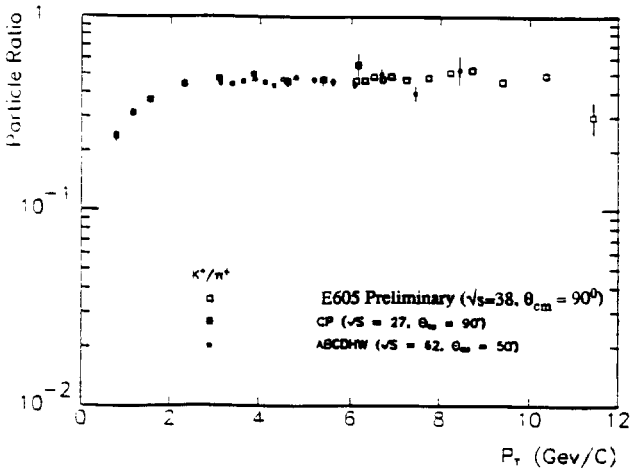


Figure 23

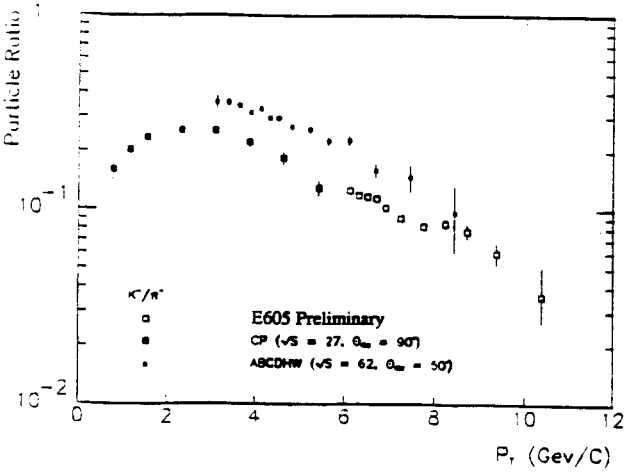


Figure 24

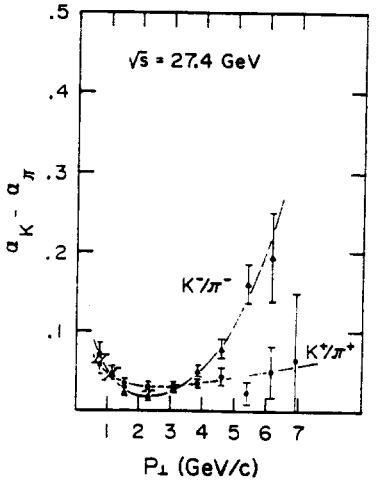


Figure 25

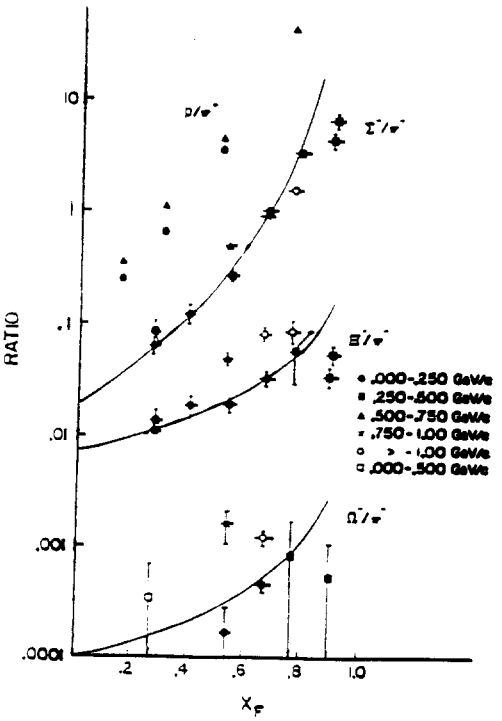


Figure 26a

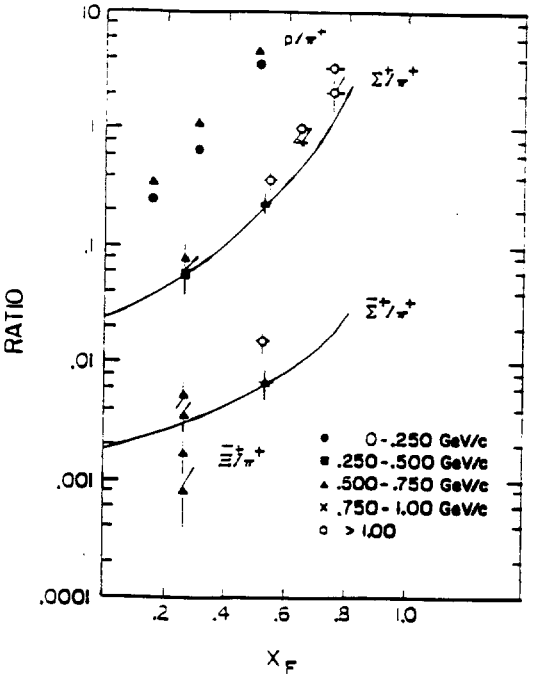


Figure 26b

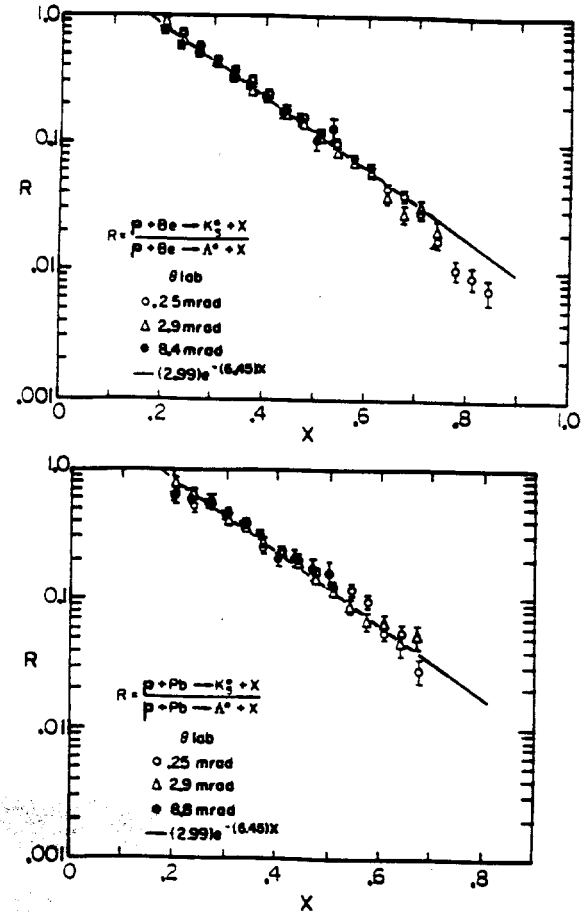


Figure 27

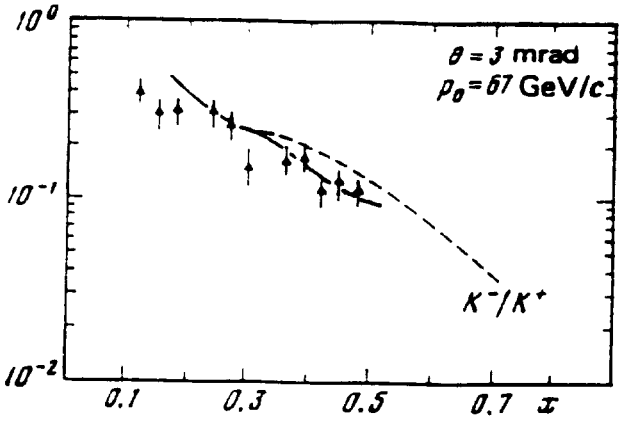


Figure 29

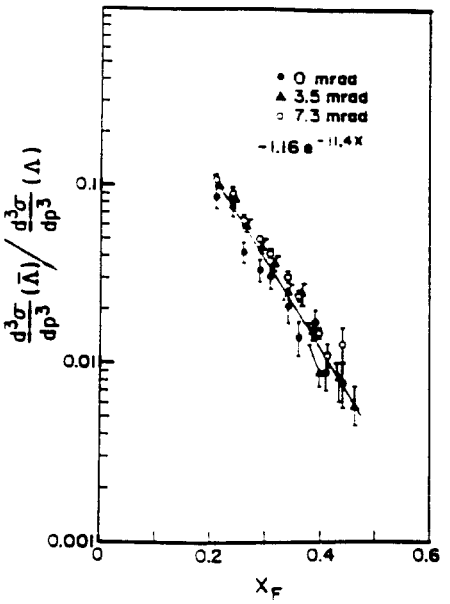


Figure 30

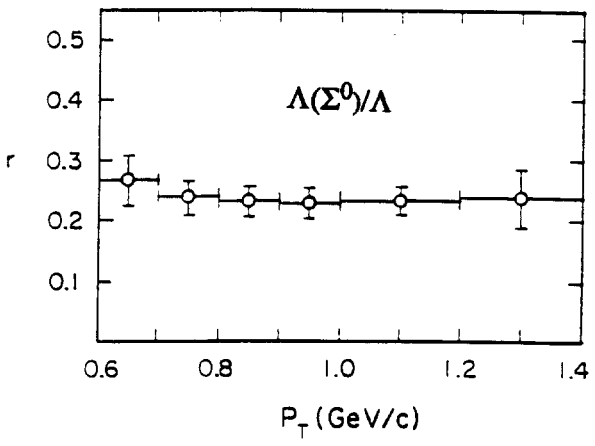


Figure 28

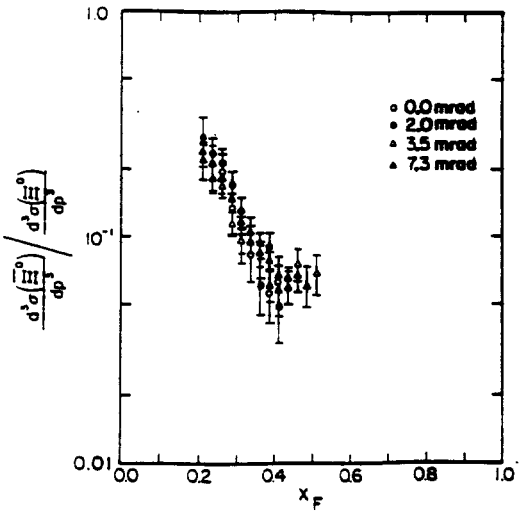


Figure 31

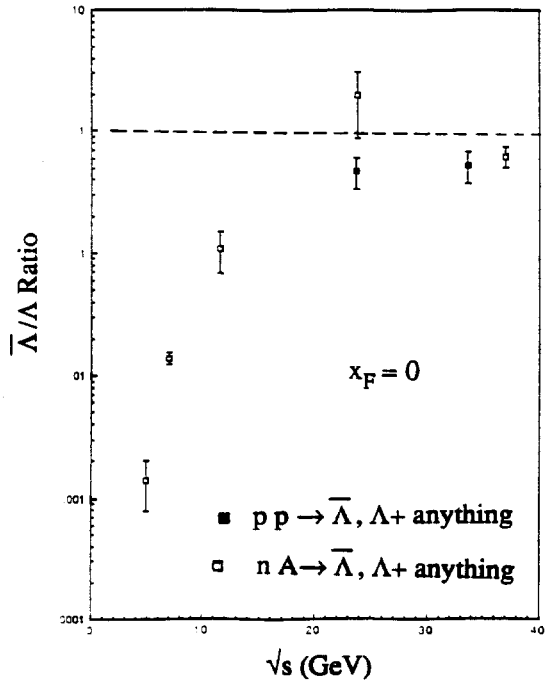


Figure 32

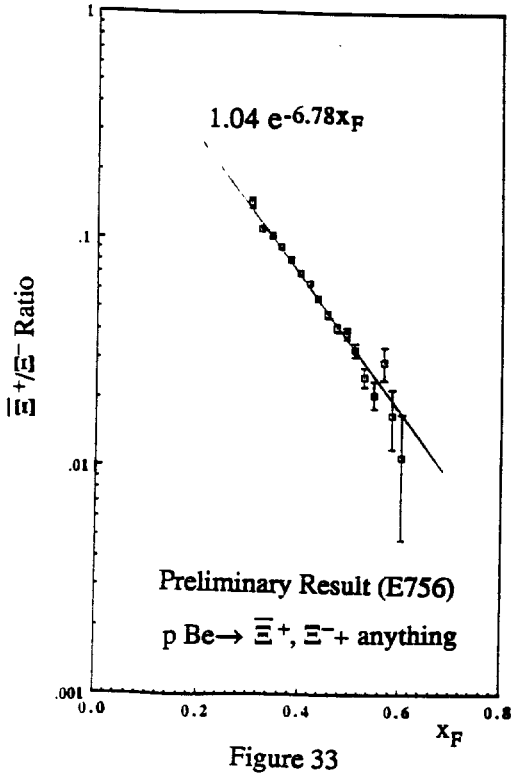


Figure 33

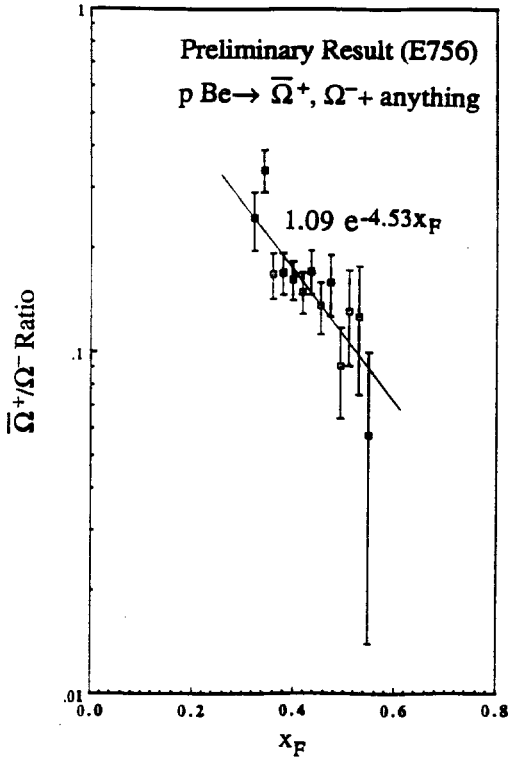


Figure 34

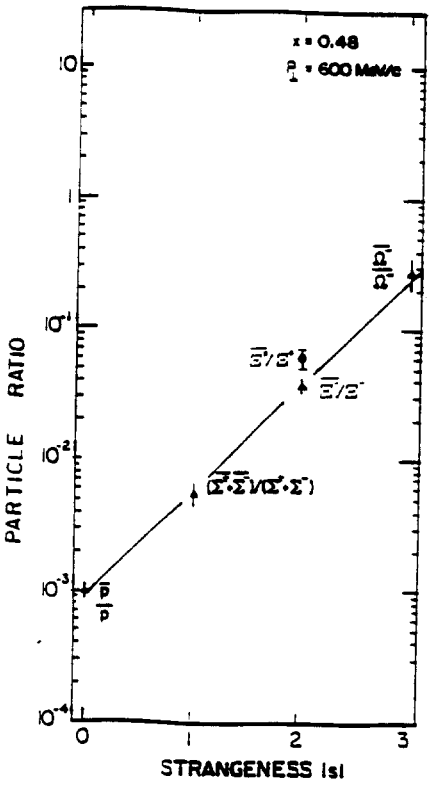


Figure 35

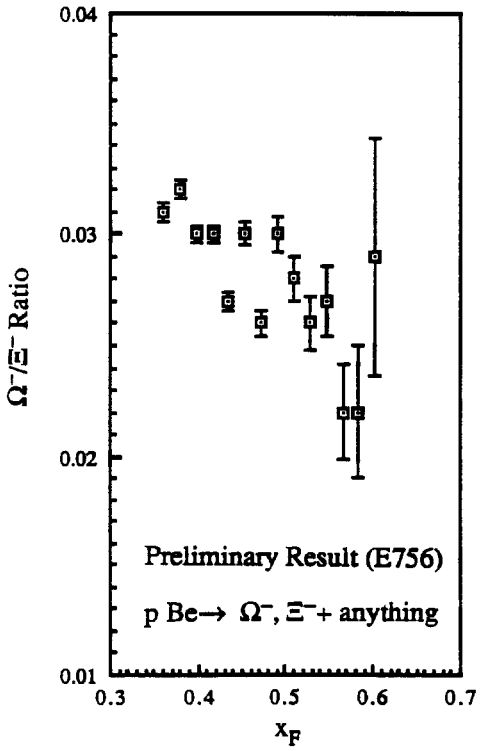


Figure 36

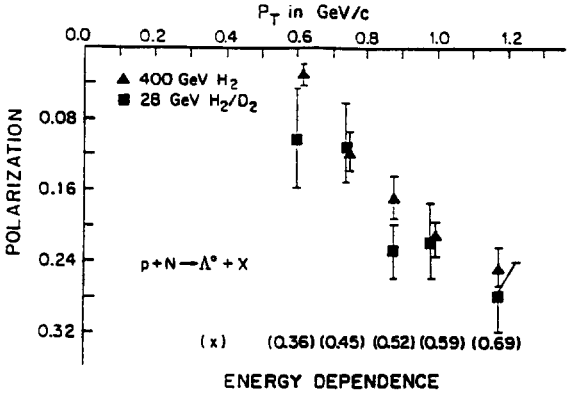


Figure 37

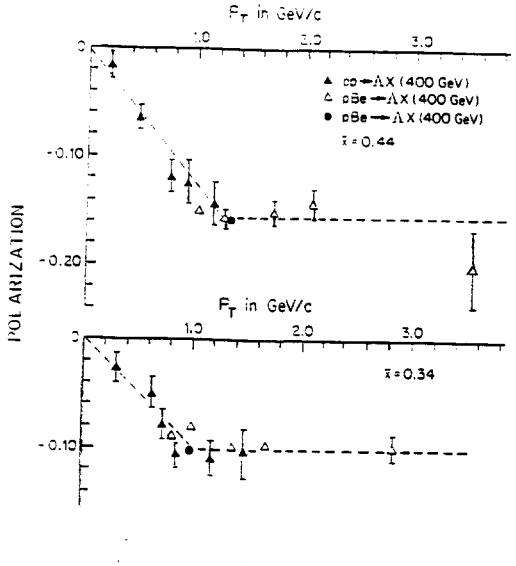


Figure 38

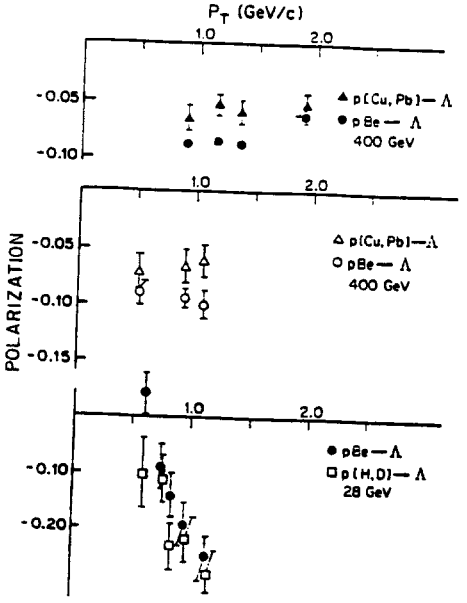


Figure 39

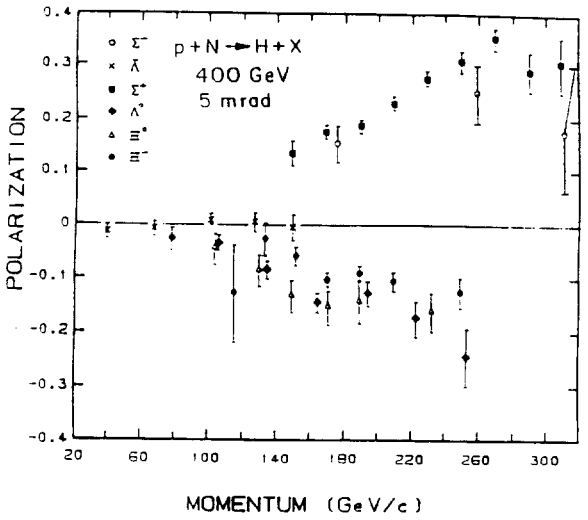


Figure 40

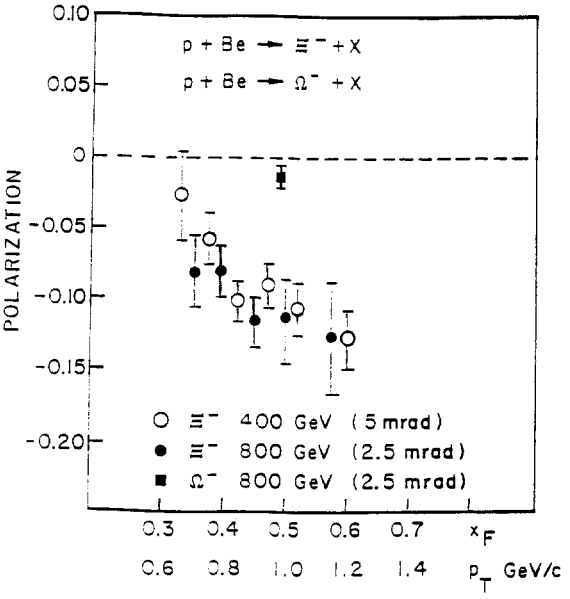


Figure 41